1008

Improvement of Laser Induced Residual Stress Distributions via Shock Waves

Wenwu Zhang and Y. Lawrence Yao
Department of Mechanical Engineering
Columbia University, New York, NY 10027

Abstract

Laser materials processing normally induces a certain residual stress distribution in the target material. Distributions favoring microcrack propagation lead to reduced fatigue life of the material. This paper investigates the feasibility of altering the stress field by using underwater shock waves in the micron scale. Shock pressure was computed and the stress analysis was conducted, in which both pressure and strain rate dependence of the plastic deformation was considered. It was shown that laser induced underwater shock waves could impart compressive stresses about 40 microns into metallic materials such as aluminum when a 12 micron laser beam was used. Experimental results of shock processing and its combination with drilling at micron scale are also presented.

1. Introduction

Since laser materials processing undergoes intensive non-uniform temperature changes in the target material, strong temperature gradients result in thermal and residual stresses around the processed areas. Unfavorable stress distributions may result in microcracks, reduce the fatigue life of processed parts, and may even cause catastrophic failures. For this reason, compressive residual stress distributions around the processed area are desired because it helps to prevent propagation of microcracks.

Thermally induced stress in laser drilling and scribing of ceramics was studied (Modest, 1997; Modest and Thomas, 1999). Their simulations show that in laser drilling, there is a very thin region of compressive residual stress at the surface of the hole, while substantial tensile stresses develop over a thick layer below and parallel to the surface. Numerical analysis of the heat affected zone and residual stress distributions for laser cutting of stainless steel was investigated (Li and Sheng, 1995; Sheng and Joshi, 1995). A 2D in-plane model was adopted, and a hybrid method for modeling heat transfer and thermal stress was introduced whereby the kerf width was determined through an analytical solution. Their simulations show that along the cutting edge there are high levels of tensile stress that sharply reverts to compressive stress once away from the edge. The sharp stress gradient was thought to make the cutting edge susceptible to micro/macro cracks.

Laser shock processing (LSP) has been studied on and off since 1970s (Clauer, et al., 1981; Peyre, et al., 1998). Laser generated shock waves in a confined medium have been used to improve the mechanical properties of various metals such as aluminum, steel and copper. LSP can induce in-depth compressive residual stress in the target and improve its fatigue life. The beam spot size used is in the order of millimeters and the compressive stress can typically reach 1 mm into the target material.

Underwater laser machining has certain attractiveness. The enhanced cooling rate of the liquid medium can help to reduce HAZ, the denser medium may help to reduce redeposition in

machining, etc. This paper investigates the possibility of laser shock processing at small scales (beam size in the order of tens of microns) and in hope that such processing can be combined with laser micromachining. The key issues are whether compressive residual stress can be imparted into a certain depth and whether laser machining can be combined with LSP at micron level beam sizes.

2. Basic principles of Laser Shock Processing (LSP)

As illustrated by Figure 1 (a), when a short and intense (>1 GW/cm^2) laser pulse is irradiated onto a metallic target, the surface layer instantaneously vaporizes into a high temperature and high pressure (1~10 GPa) plasma. This plasma induces shock waves during expansion from the irradiated surface, and mechanical impulses are transferred to the target. If the plasma is not confined, i.e., in open air, the pressure can only reach several tenth of one GPa. If it is confined by water or other media, the shock pressure can be magnified by a factor of 5 or more compared with open-air conditions (Fox, 1974). At the same time, the shock pressure lasts 2 to 3 times longer than the laser pulse duration. Most LSPs also use a coating to protect the target from thermal effects so that nearly pure mechanical effects are induced. The coating could be metallic foil, organic paints or adhesives. These coatings can modify the surface loading transmitted to the substrate by acoustic impedance mismatch effects at the coating-substrate interface, and an additional 50% increase in the peak stress values can be achieved (Peyre, et al., 1998). Pressures above 1 GPa are above the yield stress of most metals, thus plastic deformation can be induced. As a result, if the peak shock pressure is over the *HEL* (Hugoniot Elastic Limit) of the target material for a suitable time duration, compressive stress distribution in the irradiated volume can be formed (Clauer, et al., 1981).

3. Modeling

3.1 Shock pressure

Earlier modeling work on laser induced shock waves was carried out by Clauer, et al. (1981). Their model considered the non-linear coupled radiation and hydrodynamic equations governing pressure evolution at the metal surface during laser irradiation. Fabbro, et al. (1990) developed a model, which assumes that the laser irradiation is uniform and therefore shock propagation in the confining medium and the target as well is one-dimensional. This model was extended and analytical relations for plastified depth and superficial residual stresses were given (Peyer, et al., 1996). The 1-D assumption is appropriate when the size of laser beam, which typically follows a Gaussian distribution, is relatively large. The shock model in this paper made modifications to Fabbro's model to satisfy the special requirements of microscale laser shock processing. The 1-D assumption is followed but a 2-D equivalence is considered to account for the small laser spot size. Figure 1 (b) illustrates the shock model used in this paper. When plasma is formed at the interface of the solid and confining medium, its volume expands and its pressure increases and shock waves propagate into the sample and the confining medium. A portion of the incident laser intensity $I(t)$ is absorbed by the plasma as

$$I_p(t) = AP(t)I(t) \tag{1}$$

where $AP(t)$ is the absorption coefficient and t is time. Shock wave impedance is expressed as $Z_i = \rho_i D_i$, i=1,2, where ρ is density and D is the shock propagation velocity. The subscripts, 1 and 2, denote the solid and the confining medium, respectively. For instance, the impedance of aluminum is 1.5×10^7 kg/m^{2}s, and the impedance of water is 1.65×10^6 kg/m^{2}s.

Defining $Z = 2/(1/Z_1 + 1/Z_2)$ and assuming a constant fraction α of internal energy be used to increase the thermal energy of the plasma, the following relations between shock pressure $P(t)$ and plasma thickness $L(t)$ can be derived (Fabbro, et al., 1990):

$$\frac{dL(t)}{dt} = \frac{2P(t)}{Z} \tag{2}$$

$$(\frac{Z}{2} + \frac{3}{4\alpha})(\frac{dL(t)}{dt})^2 + \frac{3Z}{4\alpha}L(t)\frac{d^2L(t)}{dt^2} = I_p(t) \tag{3}$$

If $I(t)$, $AP(t)$ and α are constant, shock pressure is found to be proportional to the square root of laser intensity, and thus it is reasonable to assume that shock pressure follows a Gaussian spatial distribution with its $1/e^2$ radius proportional to that of the laser beam. In this way, spatial non-uniformity of shock pressure is considered, which is needed when the laser spot size is small as in this case. The spatially uniform shock pressure $P(t)$ relates to the spatially non-uniform shock pressure as

$$P(r,t) = P(t)\exp(-\frac{r^2}{2R^2}) \tag{4}$$

where r is the radial distance from the laser center, and R the laser beam size. $P(r,t)$ can be solved numerically from the above equations given initial values of $P(t)$ and $L(t)$. The values of $P(r,t)$ are then used as dynamic shock load in the stress analysis. Two major factors influencing shock pressure $P(t)$ are the interaction coefficient α and the intensity of the laser beam $I(t)$. A larger α results in larger pressure and longer shock wave duration as shown in Figure 2 (a). α varies from 0.1 to 0.3 while the pulse duration is kept as 50 ns. A higher laser intensity results in higher shock pressure as shown in Figure 2 (b). The laser intensity varies from 2 to 6 GW/cm^2 while α is kept as 0.2 and the pulse duration is kept as 50 ns.

3.2 Stress analysis

In LSP, the target is subjected to very strong shock pressures (>2 GPa), the interaction time is very short (<100 ns), and the strain rate is very high (>150,000 s^{-1}). A review of constitutive equations for such high strain rates was given by Meyer (1992). The simplest model describing the work hardening behavior of metals is

$$Y = A + B\varepsilon^n \tag{5}$$

where Y is the yield strength, n, A and B are material constants, and ε is the equivalent plastic strain. Eq. 5 was extended to include the influence of temperature T and strain rate $\dot{\varepsilon}$, (Johnson, et al., 1983)

$$Y = (A + B\varepsilon^n)[1 + C\ln(\dot{\varepsilon}/\dot{\varepsilon}_0)]K_T \tag{6}$$

where C is the logarithmic rate sensitivity, and K_T is a temperature related constant. The strain rate $\dot{\varepsilon}$ is normalized with a reference strain rate $\dot{\varepsilon}_0$. This model was based on experiments with strain rates from 0 to 400 s^{-1} and it did not consider pressure effects, which are very important in laser shock processing. A constitutive model applicable to ultrahigh pressures was given by Steinberg, et al. (1980):

$$G = G_0[1 + (\frac{G_p'}{G_0})\frac{P}{\eta^{1/3}} + (\frac{G_T'}{G_0})(T - 300)] \tag{7}$$

$$Y = Y_0[1 + B(\varepsilon + \varepsilon_i)]^n[1 + (\frac{Y_p'}{Y_0})\frac{P}{\eta^{1/3}} + (\frac{G_T'}{G_0})(T - 300)] \quad (8)$$

$$G_p' = \frac{dG}{dP}, G_T' = \frac{dG}{dT}, Y_P' = \frac{dY}{dP}, \frac{Y_p'}{Y_0} \approx \frac{G_p'}{G_0} \quad (9)$$

where G is the shear modulus, P is pressure, Y_0 and G_0 are values at reference state (T = 300 K, P = 0 Pa, strain free), η is the volume compression coefficient, and ε_i is the initial plastic strain (normally equals zero). Steinberg's model does not consider rate dependent effects. It was found that rate dependent effects played a minor role at pressures above 10 GPa and their rate independent model was verified to successfully reproduce shock experimental data in this range. However, for shock pressures below 10 GPa, the rate dependent effects cannot be neglected. For LSP, the pressure involved is fairly high (>1 GPa) but less than 10 GPa.

Assuming that the material compression is negligible in the range of working pressure below 10 GPa and let C be the logarithmic strain rate sensitivity at strain rate 1 s^{-1}, the following two equations are suggested.

$$G = G_0[1 + (\frac{G_p'}{G_0})P + (\frac{G_T'}{G_0})(T - 300)] \quad (10)$$

$$Y = Y_0[1 + C\ln\dot{\varepsilon}][1 + B\varepsilon]^n[1 + (\frac{Y_p'}{Y_0})P + (\frac{G_T'}{G_0})(T - 300)] \quad (11)$$

Equations 9 to 11 are the stress-strain relations used in this paper. This model is valid for $\dot{\varepsilon} > 10^{-6}$ s^{-1}. Below this strain rate, quisistatic experimental data should be used. In simulation, the following parameters for pure aluminum are used: G_0 = 27.6 GPa, Y_0 = 70 MPa, B = 125, C = 0.01, n = 0.2, $G'_p/G_0 = Y'_p/Y_0 = 6.5\times10^{-11}$ Pa^{-1}, $G'_T/G_0 = -6.20\times10^{-4}$ K^{-1}. Given these parameters, Y at any given set of P, T, ε and $\dot{\varepsilon}$ can be computed.

Figure 3 (a) illustrates the increase of yield strength with the increase of strain rate at different strains with zero pressure and T = 300 K. It is clear from this Figure that rate dependence is strong. The model of Steinberg overestimates the yield strength at low strain rates, and underestimates the yield strength at strain rates bigger than 1. Figure 3 (b) shows the influence of pressure on the yield strength, the strain rate is kept at 1. Below 0.1 GPa, the influence of pressure is negligible. Obvious increase of yield strength with pressure starts at around 1 GPa (6.5%), and the yield strength has increased 32.5% at 5 GPa. In the range of 1 GPa to 5 GPa, the increase of yield strength from shock pressure effects is more important than but still comparable to that from strain rate effects, so neither of them can be neglected.

In the following stress analysis, work hardening, strain rate and pressure are considered while temperature is taken as room temperature. This is reasonable because only the coating is vaporized and minimal thermal effects are felt by the sample. Shock pressure is first computed and used as loading for the stress analysis. A commercial FEM software, ABAQUS, is used to compute the stress distribution and deformation of the sample under the shock pressure. The computation domain is 50 microns in y-direction and 100 microns in r-direction (Figure 1b). The mesh is denser near the center and the top. Grid number is 25 in y-direction and 50 in r-direction. The simulation is divided into two steps. Step one is a dynamic implicit nonlinear process and the step time is chosen 150 ns justified by results shown in Figure 2. The spatial and temporal dependent shock load is applied on the nodes within 1.5 times of the laser beam size. Outside this

range the top surface of the solid is treated as traction free. Step 2 is also a dynamic implicit nonlinear process and the step time is chosen 1ms to let the process to complete. In this step the shock load is removed and the shock induced stress relaxes. Let the displacements in the r and y directions be d_r and d_y respectively, the boundary conditions for the axisymmetric stress model are as follows. At the centerline, symmetric constraints: $d_r = 0$; At the outer edge, traction free: $\sigma_{ij}n_j = 0$, $i,\ j = r, y$; At the bottom surface, zero displacements in y-direction: $d_y = 0$; At the top surface, surface traction equals applied shock pressure: $\sigma_{ij}n_j = P(r,t),\ \ i, j = r, y$.

3.3 Considerations for combining LSP with laser micro-machining

Considerations have been given in choosing a suitable range of laser intensity if LSP is to be combined with laser micro-machining. For LSP, the peak shock pressure should lie between 1*HEL* and 2*HEL* of the target material to be able to generate plastic deformation but to prevent detrimental effects on the target (Peyre, et al., 1996). To obtain deep compressive residual stress, the shock pressure should be close to 2*HEL*. There is no need to concern the breakdown of water since LSP is normally carried out using a single or few pulses. If machining is to be incorporated, which normally requires a pulse train, one has to ensure the laser intensity is below the strong breakdown intensity of water. Otherwise, the water breakdown will take place during the subsequent pulses and water will lose its function of confinement. The strong breakdown intensity of water is about 6 GW/cm^2 for the 355 nm wavelength (Berthe, et al., 1998). Taking this factor into account, laser intensity of 2 to 4 GW/cm^2 is suggested for possible combination of LSP and laser micromachining. This range of laser intensities enables efficient machining and at the same time generates shock pressures greater than the *HEL* of most metals to induce substantial compressive residual stresses. Beam intensity distribution, which have been considered in equation (4), heat transfer and changing geometry of the sample should also be considered in laser micro-machining but beyond the scope of this paper.

4. Simulation results and discussions

When laser shock is applied on the top surface of the sample, the sample undergoes a transient movement. The shock load is computed at $I = 4$ GW/cm^2, $\alpha = 0.2$, $AP = 0.5$, thus the actual shock pressure is equal to the $I = 2$ GW/cm^2 curve in Figure 2 (b) whose peak pressure is 1.88 GPa. Figure 4 (a) illustrates the accelerations in the y-direction of four centerline points *P1, P2, P3* and *P4* which are 1.057, 2.337, 3.889 and 14.146 microns below the top surface, respectively. In order to see the transient response in a large time range, the time axes used log coordinates. The acceleration curves clearly indicate the propagation of the shock waves--the quick increase of accelerations at different locations starts at different time. The points near the top surface have stronger movements than those far away, the movement settles down at $t = 1.5$ μs, which is about 10 times of the shock duration (150 ns). The wavelets in the curves are attributed to bounce back and forth of the lattice from the equilibrium position under the influence of the shock waves. The two large peaks of *P1* are (0.45 ns, -7.473×10^9 m/s^2) and (37.69 ns, 1.46×10^{10} m/s^2). Simulation also shows that the peak velocities of the four points are reached at around $t = 26$ ns, location makes little difference although their peak values are different. The largest peak velocity reaches -137 m/s at *P1*. Displacements of the four points increase until $t = 45$ ns, after that, relaxation occurs, the displacements bounce back a little. The peak displacement of *P1* is -3.5148 microns.

The movements in the y-direction of other areas have similar features as those of the centerline points and their motions are nearly synchronized if they are at the same height. The motion in the

r-direction is weaker than the motion in the *y*-direction. The peak velocity in the *r*-direction is less than 5 m/s, displacement is less than 80 nm, the peak acceleration is less than 1.75×10^9 m/s^2 and the motion also settles down at around 1.5 μs.

Strain rate effects are important for laser shock processing. The evolution of the equivalent plastic strain is shown in Figure 4 (b) for the above mentioned four points. Plastic strain develops quickly from 20 ns to 30 ns. This is the period when the shock pressure is the highest. The strains smooth off after $t = 30$ ns and changes very little after $t = 50$ ns. The plastic strain of element *P2* reaches 0.28 at $t = 45$ ns and this equals an average strain rate of 6.22×10^6 s^{-1}.

Figure 5 shows the simulation results of the distributions of radial and circumferential residual stresses *S11* and *S33*. The radial stress *S11* is compressive in the area nearly 45 microns below the surface and 80 microns in diameter as shown in Figure 5 (a). Near the edge of laser irradiated region, there exists a thin layer (<2 μm) of tensile stress distribution. The largest compressive stress is 174.25 MPa, while the largest tensile stress is only 53.77 MPa. The circumferential residual stress distribution *S33* is shown in Figure 5 (b). The compressive region of *S33* has an expanding spherical shape, the high compressive stress is located at 10 microns below the center point and the largest stress is 174.25 MPa. A tensile region circumferences the center compressive region. Similar to *S11*, a tensile area exists near the top edge of the laser shocked region. Simulation also shows that the *y*-direction stress *S22* is relatively weak compared with *S11* and *S33*. *S22* is compressive in the region below the irradiation area for a depth of 35 microns and the maximum value is -57 MPa at 23 microns below the center point. Simulation shows that a dent is formed at the shocked area, which is verified by experiments.

Such stress distributions are very different from the open-air results given by Modest (1997), which shows a thin layer of surface compressive residual stress and a large volume of tensile stress below the surface. From the above simulation and experimental results, it is shown that compressive residual stress exists in a wide region in the *y* (*S22*), radial (*S11*) and circumferential (*S33*) directions. *S11, S22* and *S33* being compressive are important for preventing radial and circumferential crack formations.

5. Experiment results and discussion

Al 1100 foil of 70 micron thickness was used as samples. The samples were polished and the sample size was about 5 mm square. To apply the coating, a thin layer of high vacuum grease (about 10 microns) was spread evenly on the polished sample surface, and the coating material, aluminum foil 16 microns thick, was then pressed onto the grease. The sample was placed in a shallow container and distilled water was filled until the water above the sample was around 3 mm (Figure 1a). The box was placed on a XYZ table so that the *z*-direction focusing and *x*/*y*-direction positioning can be conveniently controlled. A frequency tripled Nd:YAG laser generating TEM00 Gaussian beam was used, the pulse duration was 50 ns, pulse repetition rate could vary between 1 Hz to 20 KHz. Laser beam size is about 12 microns. After shock processing, the coating layer and the vacuum grease were removed. Besides shocking experiments, multiple pulses were used, which not only shocked the sample but also left holes on the samples to obtain initial experience to combine LSP with laser micro-machining. These samples were examined using SEM.

Figure 6 (a) shows the SEM pictures of laser shock induced dents on the aluminum sample by three laser pulses. The laser intensity is 4 GW/cm^2. These dents are direct evidence of plastic deformations on micron scales. Figure 6 (b) shows a hole drilled underwater with a 16 micron thickness aluminum coating layer on the 70 micron thickness aluminum sample, 45 laser pulses at

4 GW/cm^2 were used. The SEM picture was taken at 45 degrees. There is a large dent around the hole. The wall surface of the hole is smooth and shows signs of compression. Compared with open air drilling, the taper is small and the redeposition around the hole is greatly reduced.

6. Conclusions

Laser shock processing at microns level for the purpose of residual stress distribution improvement was discussed in this paper. A 2D axisymmetric model for shock pressure computation was given and the computed shock pressure was used as the dynamic load in stress analysis. Ultrahigh strain rate effects on plastic deformation were considered and a constitution relation taking into account of strain rate, pressure, temperature and work hardening effects were given. It was shown that compressive residual stress as high as 170 MPa could be generated using micron level beam sizes at 355 nm wavelength. Both simulation and experiments show that large regions of plastic deformation are achievable around the laser shocked area. The potential of combining LSP with underwater laser micro-machining was also shown.

7. Acknowledgements:

Financial support from NSF under grant DMI-9813453 and equipment support from ESI are gratefully acknowledged. Assistance with SEM measurements rendered by Dr. Alex Limanov is appreciated.

8. References

Berthe, L., et al., 1998, "Experimental study of the transmission of breakdown plasma generated during laser shock processing," *The European Physical Journal Applied Physics*, 1998, Vol. 3, pp 215-218.

Clauer, A. H., et al., 1981, "Effects of laser induced shock waves on metals," Shock Waves and High Strain Phenomena in Metals-Concepts and Applications, New York, Plenum, 1981, pp. 675-702

Fabbro, R., et al., 1990, "Physical study of laser-produced plasma in confined geometry," *J. Appl. Phys.*, July, 1990, Vol. 68(2), pp. 775-784.

Fox, J. A., 1974," Effect of water and paint coatings on laser-irradiated targets," *Appl. Phys. Lett.*, 15 May 1974, Vol.24, No. 10, pp. 461-464.

Johnson, G. R., et al., "Response of various metals to large torsional strain over a large range of strain rates," *J. Eng. Mat. Techn.*, Jan. 1983, Vol. 105, pp. 42-53.

Li, K. and Sheng, P. S., 1995, "Computational model for laser cutting of steel plates," *Manufacturing Science and Engineering*, ASME 1995, MED-Vol. 2(1), pp.3-14.

Meyer, L. W., 1992, "Constitutive equations at high strain rates," Shock-wave and High-Strain-Rate Phenomena in Metals, Marcel Dekker, Inc., New York, 1992, pp. 49-68.

Modest, M. F., 1997, "Thermal elastic and viscoelastic thermal stresses during laser drilling of ceramics," *J. Heat Transfer*, 1997, Vol. 120, pp. 892-898.

Modest M. F., and Mallison, T. M., 1999, "Transient elastic thermal stresse development during laser scribing of ceramics," *ICALEO 1999*, pp. B118-127.

Peyre, X. S., et al., 1998, "Current trends in laser shock processing," *Surface Engineering*, 1998, Vol. 14 No. 5, pp. 377-380.

Peyre, P., et al., 1996, "Laser shock processing of materials, physical processes invloved and examples of applications," *Journal of Laser Applications*, 1996, Vol. 8, pp.135-141.

Sheng, P. S. and Joshi, V. S., 1995, "Analysis of heat-affected zone formation for laser cutting of stainless steel," *Journal of materials Processing Technology*, 1995, Vol. 53, pp. 879-892.

Steinberg, D. J., et al., 1980, "A constitutive model for metals applicable at high-strain rate," *J. Appl. Phys.*, March 1980, Vol. 51(3), pp. 1498-1504.

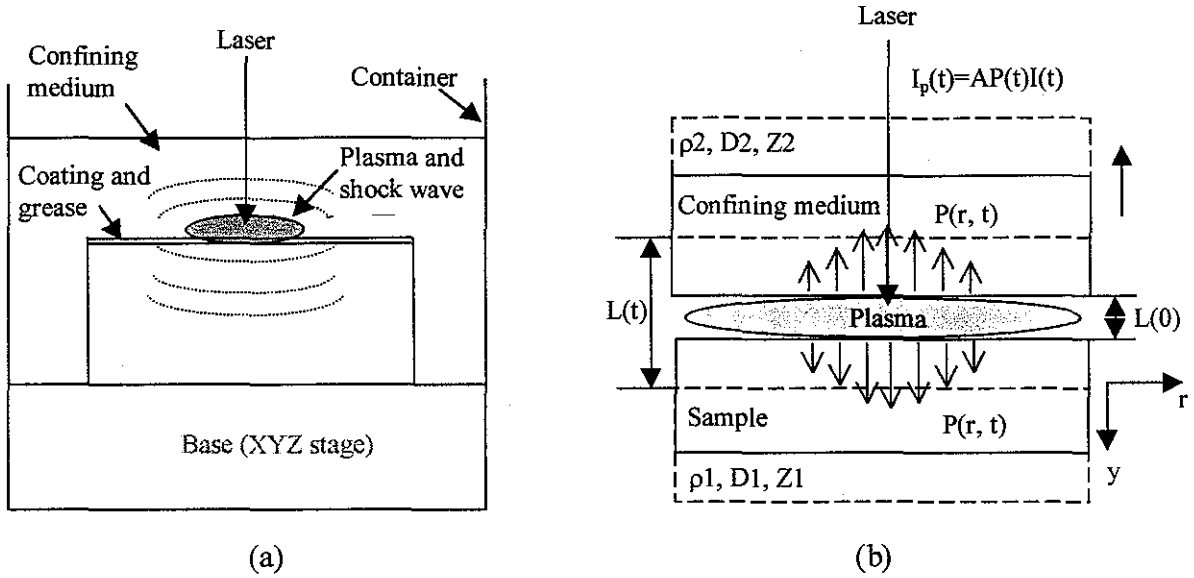

Figure 1 (a) Principles of laser shock processing (LSP); and (b) Illustration of LSP modeling. Axisymmetry (*r, y)* is assumed.

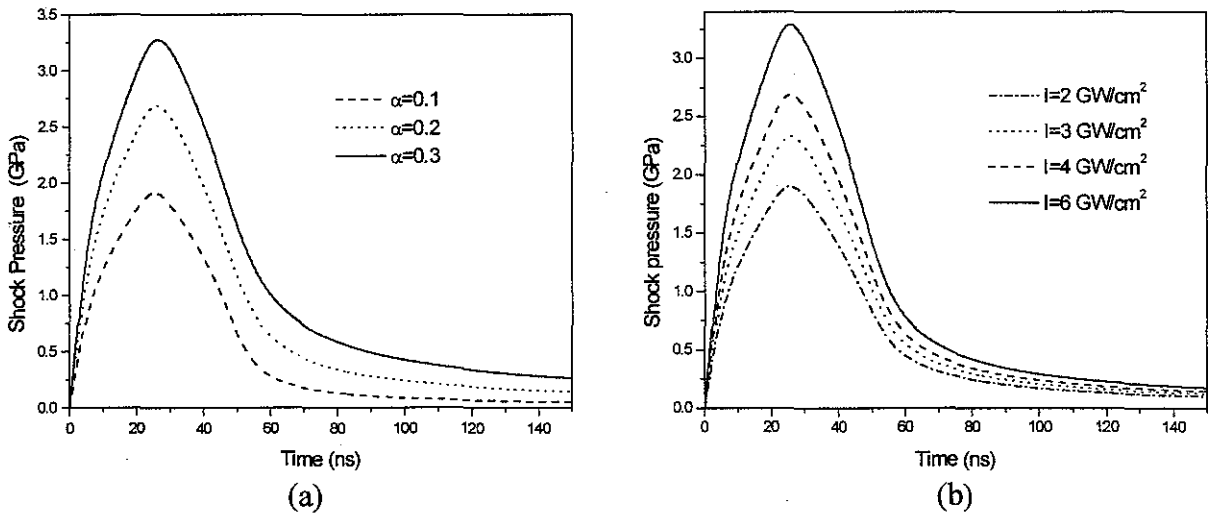

Figure 2 (a) Effects of plasma absorption coefficient α on shock wave pressure (laser pulse duration is 50ns and laser intensity is I=4GW/cm^2); and (b) Effects of laser intensity on shock wave pressure (laser pulse duration is 50ns and α=0.2).

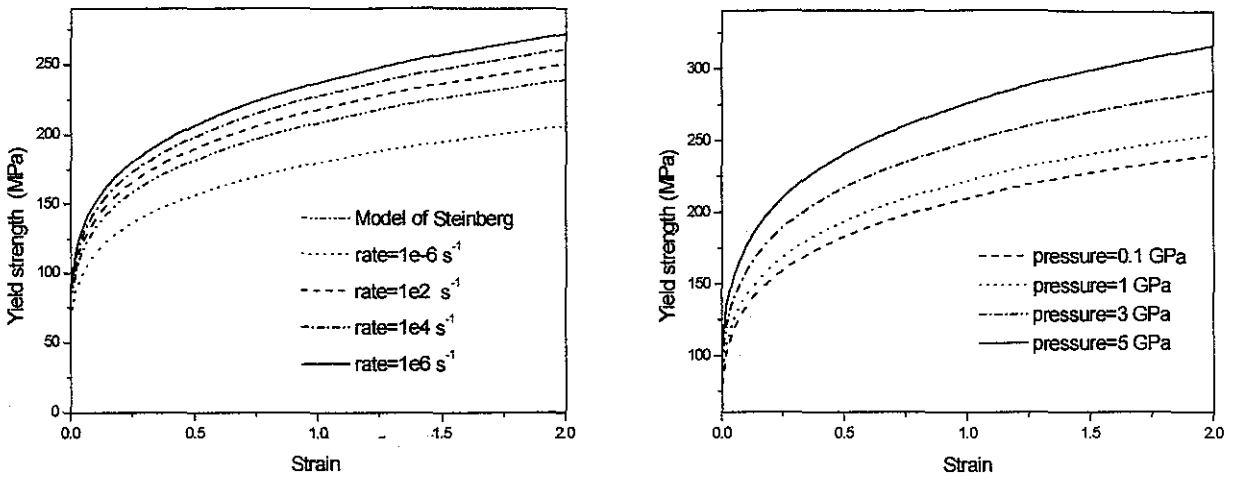

(a) (b)

Figure 3 (a) The influence of strain rate on the yield strength (zero pressure and T=300K); and (b) The influence of pressure on the yield strength (strain rate=1 s^{-1} and T=300K).

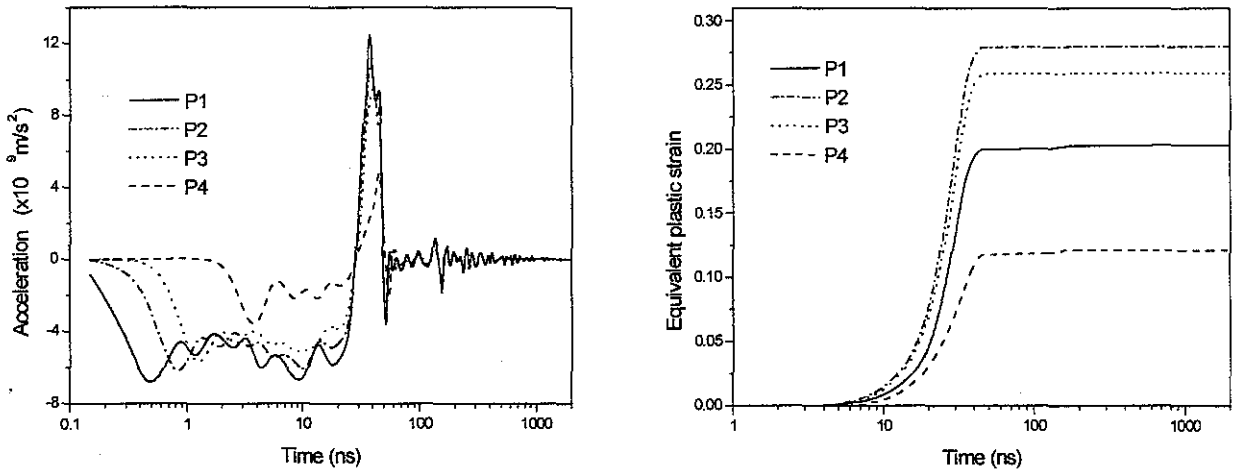

(a) (b)

Figure 4 (a) Solid particle acceleration in the y-direction (depth direction); and (b) Equivalent plastic strain in the same direction (*P1, P2, P3* and *P4* are points 1.057, 2.337, 3.889 and 14.146 microns below the center point on the top surface of the solid, respectively, I=2GW/cm^2).

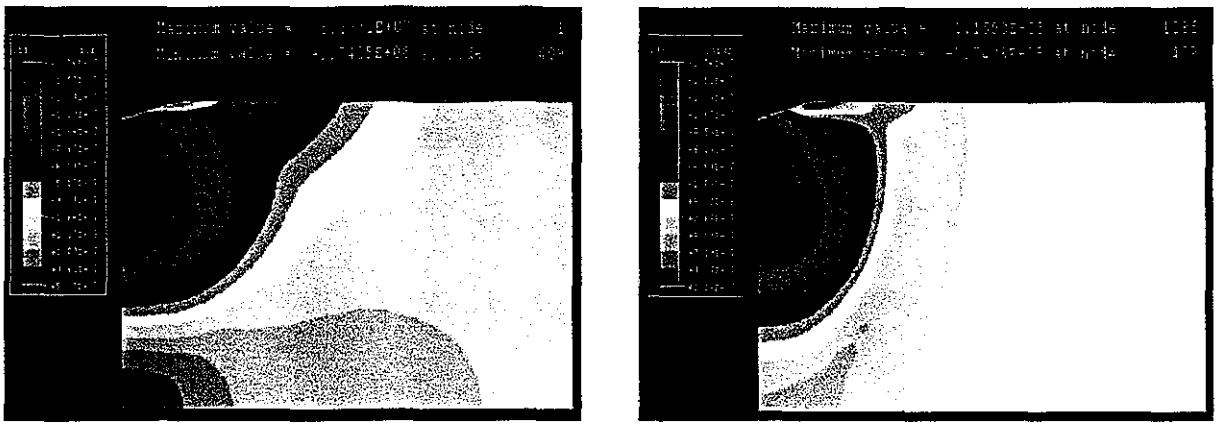

(a) (b)

Figure 5 (a) Distribution of radial residual stress *S11*; and (b) Distribution of circumferential residual stress *S33* (I=4GW/cm^2, α=0.2, AP=0.5, and laser beam radius R=6 microns). Half of the target is shown due to symmetry. The computation domain is 50 microns in the y-direction and 100 microns in the r-direction.

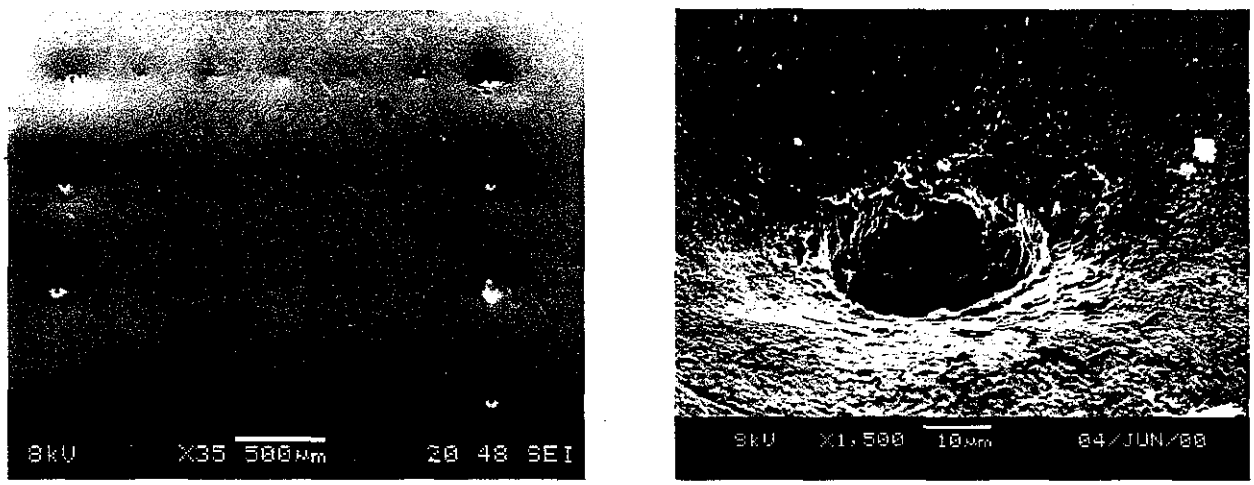

(a) (b)

Figure 6 (a) SEM micrograph of dents induced by laser shock processing (3 pulses) and holes (45 pulses), and (b) close-up view showing that the area surrounding the drilled hole is also dented. (Al 1100 foil 70microns thick, aluminum coating layer 16 microns thick; laser wavelength 355 nm, pulse duration 50 ns, intensity 4GW/cm^2, spot size12 microns, and repetition rate 1KHz).

Meet the authors

Wenwu Zhang is currently a Ph.D. candidate and Y. Lawrence Yao an Associate Professor in the Department of Mechanical Engineering at Columbia University, where Yao also directs the Manufacturing Engineering Program. Yao has a Ph.D. from Univ. of Wisconsin-Madison.